

# Symmetry-preserving momentum remap for ALE hydrodynamics

J Velechovský<sup>1</sup>, M Kuchařík<sup>1</sup>, R Liska<sup>1</sup> and M Shashkov<sup>2</sup>

<sup>1</sup>Czech Technical University, Faculty of Nuclear Sciences and Physical Engineering, Břehová 7, Praha 1, 115 19, Czech Republic

<sup>2</sup>Los Alamos National Laboratory, Group XCP-4, Los Alamos NM 87545, USA

E-mail: [velecjan@fjfi.cvut.cz](mailto:velecjan@fjfi.cvut.cz)

**Abstract.** In this paper, a symmetry-preserving remapping algorithm for vectors respecting their local bounds by components and in magnitude is presented. First, description of the Vector Image Polygon (VIP) limiter for a piece-wise linear velocity reconstruction is presented. Numerical fluxes obtained from this reconstruction lead to symmetry- and bounds- preserving remap of momentum for staggered Arbitrary Lagrangian-Eulerian (ALE) hydrodynamical methods. A novel bounds definition for vectors and corresponding modification of the VIP limiter is introduced, which fixes undershoots in a radial velocity component for polar meshes. Comparison with standard scalar-based limiters is given. Cyclic remapping is performed to numerically verify properties of the methods.

## 1. Introduction

The Arbitrary Lagrangian-Eulerian (ALE) [1] methods became a standard and successful approach in the hydrodynamic codes for laser generated plasmas. In our 2D code Prague ALE (PALE) [2], we are able to perform simulations of high-velocity plasma flows generated by an intense laser beam. PALE code incorporates a staggered discretization of the hydrodynamic equations, in which the thermodynamic quantities are located in the computational cells while the kinematic quantities are located on the nodes of the mesh. A typical ALE method can be divided in three steps: 1) the Lagrangian solver; 2) mesh relaxation; and 3) the remapping method interpolating conservatively all fluid quantities between the meshes. Many production codes employ the ALE machinery, next to our PALE code, let us name CHIC [3], CORVUS [4], FLAG [5], ALEGRA [6], or ALE-AMR [7].

Standard limiters for a scalar are usually applied for Cartesian components of vectors during the remapping stage. Symmetry-preserving vector remapping methods use the VIP limiting procedure [8] or the projection of the velocity in the principal flow direction [9].

## 2. Remapping overview

Suppose that we have two computational meshes – an old (Lagrangian) mesh  $\{c\}$  and a new (rezoned) mesh  $\{\tilde{c}\}$ . Let us assume that both meshes have the same connectivity and are close to each other. The remap of mass (for example) can be written in the following flux form

$$m_{\tilde{c}} = m_c + \sum_{c' \in C'(c)} F_{c,c'}^m, \quad (1)$$



where  $C'(c)$  represents a set of all cells neighboring with cell  $c$ , and  $F_{c,c'}^m$  stands for the (outwards oriented) mass flux from  $c$  to  $c'$ . Depending on the particular remapping method, the  $F_{c,c'}^m$  fluxes can be constructed in different manners. In our approach, integration of the density function over all intersections of the original cell  $c$  with all its neighbors in the new mesh is used [10].

For nodal mass, we employ remap in a flux form analogous to (1),

$$m_{\tilde{n}} = m_n + \sum_{n' \in N'(n)} F_{n,n'}^m, \quad (2)$$

where  $N'(n)$  stands for the set of nodes neighboring with node  $n$ , and  $F_{n,n'}^m$  represents the inter-nodal mass flux from  $n$  to  $n'$ . In the formula, we only consider one flux per neighbor, which can in practice be split in two parts corresponding to the different attached cells.

Exact integration by intersecting the dual cells of old and new mesh is computationally expensive due to generally non-convex dual cells. One possibility is the cheap interpolation of the inter-nodal mass fluxes  $F_{n,n'}^m$  from the inter-cell ones in a way similar to the one described in [11].

For remap of nodal momentum vector, formula analogous to (2) is used. This remap can be rewritten for nodal velocity  $\vec{w}_n$  as

$$\vec{w}_{\tilde{n}} = \frac{1}{m_{\tilde{n}}} \left( m_n \vec{w}_n + \sum_{n' \in N'(n)} \vec{F}_{n,n'}^\mu \right). \quad (3)$$

The new nodal mass  $m_{\tilde{n}}$  is already known (2) and the momentum fluxes  $\vec{F}_{n,n'}^\mu$  can be obtained in several ways. We prefer reusing the computed mass fluxes  $F_{n,n'}^m$ , and constructing the momentum fluxes by their multiplication by the reconstructed velocity vector,  $\vec{F}_{n,n'}^\mu = F_{n,n'}^m \vec{w}_{n,n'}$ , which is consistent with the DeBar condition [12].

Our goal is to develop momentum remapping method which is symmetric and preserves bounds on a polar grids for radial velocity field and radial grid motion. In this pseudo-1D case, we want to keep velocity vector in limits given by standard 1D bounds for its radial component (note that the angular component is 0 for the symmetric case). This is equivalent to bounds in velocity magnitude for a special case where radial velocity does not change direction along a ray from an origin, e.g. purely convergent or divergent velocity field. This property is not satisfied by standard approaches for velocity reconstructions.

### 3. Velocity reconstructions

Let us remind notation for variables on our staggered logically orthogonal quadrilateral mesh. We denote cell quantities (such as cell center  $x_c$ ) by integer subscript  $c$  and nodal, e.g. node position  $\vec{x}_n$  or velocity  $\vec{w}_n$ , by subscript  $n$ . A cell  $c$  is defined by a set of its nodes  $N(c)$ . Similarly, a node  $n$  is shared by a set of cells  $C(n)$ .

#### 3.1. Piecewise constant velocity reconstruction

This reconstruction imitates the cell-based donor remapping method. A particular node is chosen with respect to the sign of an inter-nodal mass flux, which is given by the grid movement. Imagine that we have mass flux  $F_{n,n'}$  from node  $n$  to  $n'$  given in some point  $\vec{x}$ . Then, the reconstructed velocity  $\vec{w}_{n,n'}$  has the form

$$\vec{w}_{n,n'} = \begin{cases} \vec{w}_n & \text{for } F_{n,n'} > 0 \\ \vec{w}_{n'} & \text{for } F_{n,n'} < 0. \end{cases} \quad (4)$$

Resulting remapping satisfies both conditions for symmetry and bounds preservation. However, it is only first order accurate and therefore too diffusive.

### 3.2. Piecewise linear velocity reconstruction

There are many ways how to construct high-order velocity reconstruction, which are almost equivalent in regions with sufficiently smooth velocity field. Our choice of piecewise linear reconstruction on a dual mesh is motivated by the fact, that we want to approach the low-order piecewise constant reconstruction by setting a slope limiter value to zero in regions near shocks. The piecewise linear reconstruction in node  $n$  is given by

$$\vec{w}_{n,n'} = \vec{w}_n + \phi_n(\nabla\vec{w})_n(\vec{x} - \vec{x}_n) \quad (5)$$

where  $\vec{x}_n$  and  $\vec{w}_n$  are nodal position and velocity,  $\vec{x}$  stands for approximate flux position and  $\phi_n \in (0, 1)$  for a slope limiter. Unlimited slopes in velocity gradient  $(\nabla\vec{w})_n$  are computed from velocities in eight neighboring nodes using Green formula. This unlimited reconstruction (for  $\phi_n = 1$ ), as well as resulting remapping, is also symmetric. However, it produces a new extrema near shocks. Limitation is therefore necessary.

### 3.3. Barth-Jespersen limiter for piecewise linear reconstruction

This limiter for scalars was introduced in [13]. In most of recent approaches, x- and y-components of velocity  $\vec{w} = \begin{pmatrix} w^x \\ w^y \end{pmatrix}$  are limited separately with constrains

$$\begin{aligned} w_n^{x,\min} &\leq w_n^x(\vec{x}_m) \leq w_n^{x,\max} \\ w_n^{y,\min} &\leq w_n^y(\vec{x}_m) \leq w_n^{y,\max} \end{aligned} \quad \forall m \in N(C(n)), \quad (6)$$

where  $w_n^x(\vec{x}_m)$  and  $w_n^y(\vec{x}_m)$  are components of reconstructed velocity given by (5) and e.g.  $w_n^{x,\min}$  is minimal velocity component from set given by 8 neighboring nodes of node  $n$  and the node  $n$  (this set is denoted by  $N(C(n))$ ).

Let us make a short note on the scalar limiter  $\phi_n$  in (5). To limit the velocity components separately, it is common to replace the scalar by a diagonal matrix. This diagonal matrix with different limiters for velocity components was also used in our numerical tests. However, regardless of the choice of scalar or matrix form, these methods are neither symmetric nor bounds preserving for radial problems as defined at the end of section 2, because its limiter value is angularly dependent (even for the usual technique of a common limiter value taken as the minimum of both Cartesian components).

## 4. Bounds for velocity vector

Remaining question is how to compute the nodal limiter values  $\phi_n \in (0, 1)$  in (5). Similarly as in [8], we divide this question in two parts. First, how to define bounds for vector, and second, how to compute the optimal value of  $\phi_n$  to keep reconstructed vector in the bounds. This bounds definition has to be general for any field. However, we want to satisfy conditions for radial velocity on a polar mesh as mentioned above. To be illustrative, we start with comment on the Barth-Jespersen approach applied in a standard way, component by component.

Any given set of velocity bounds defined by BJ-limiter represents a rectangle (which can degenerate to a line or a point) in the velocity space (where velocity vectors are expressed by their x- and y- components), as shown in figure 1 (a, b). However, this rectangle is not invariant with respect to rotation of the coordinate system. Just compare figure 1 (a) with (b) for the same set of velocities in rotated coordinate system. It leads to violation of symmetry in our first test case for polar grids with radial velocity, see figure 2. This situation can be clearly understood by the fact that limiter moves reconstructed velocities inside the bounds represented by the angularly dependent rectangle, so the limiter value and the therefore velocity reconstruction as well as resulting remap show angular dependency even for symmetric problems. One way how to remove this dependency on Cartesian components is to switch to local coordinate system given e.g. by the principal flow direction [9, 14].

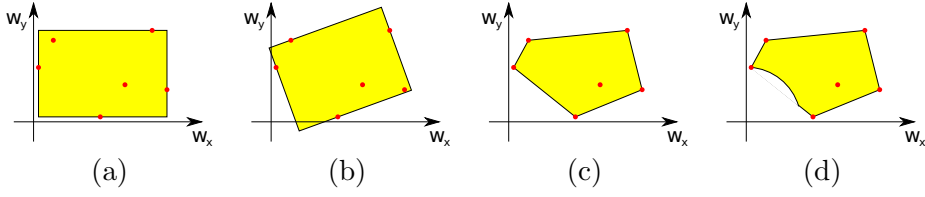


**Figure 1.** Yellow objects represent different bound definitions for 6 velocities given by red dots. (a, b) corresponds to BJ applied component by component, (c) VIP approach and (d) our modification (MVIP) of these bounds.

### 5. Vector Image Polygon approach

In [8], another definition of vector bounds is presented, which is independent of rotation of the coordinate system. These bounds are defined by the Vector Image Polygon (VIP), defined as the convex hull of a given set of velocities, see figure 1 (c). Compared to the BJ limiter applied component by component, VIP is more restrictive, because this convex hull of given velocities is equal to common intersection of all rectangles from BJ bounds for all arbitrary rotations of the coordinate system.

Our particular implementation for logically orthogonal quadrilateral mesh is slightly different from the usual approach (6). For BJ approach, we require to keep reconstruction in all neighboring nodes in the common bounds given by velocities from the same set of nodes. On the contrary for the VIP approach, we evaluate unlimited reconstruction in all cell centers around the node. For every particular cell center, we want to keep this reconstruction in limits given by nodes of the cell.

The next section describes in detail computation of the nodal limiter value  $\phi_n$ . To determine its value, we evaluate the unlimited reconstruction in four cell centers  $\vec{x}_c$  around the node

$$\vec{w}_{nc}^{\text{unlim}} = \vec{w}_n + (\nabla \vec{w})_n (\vec{x}_c - \vec{x}_n). \quad (7)$$

For every cell center  $\vec{x}_c$ , we want to find  $\phi_{nc}$  to keep reconstructed velocity

$$\vec{w}_{nc}^{\text{lim}} = \vec{w}_n + \phi_{nc} (\nabla \vec{w})_n (\vec{x}_c - \vec{x}_n) \quad (8)$$

in VIP bounds of its four nodes  $n \in N(c)$ , so we require

$$\forall c \in C(n) \quad \vec{w}_{nc}^{\text{lim}} \in \text{VIP}_c \quad (9)$$

where  $\text{VIP}_c$  represents the Convex Hull of nodal velocities  $\vec{w}_n$ ,  $n \in N(c)$ . At first, for a particular cell  $c$  attached to node  $n$  find the maximal  $\phi_{nc} \in (0, 1)$  which keeps  $\vec{w}_{nc}^{\text{lim}}$  inside  $\text{VIP}_c$ . Let us call these  $\phi_{nc}^{\text{VIP}}$  and  $\vec{w}_{nc}^{\text{VIP}}$ . Having computed all four  $\phi_{nc}^{\text{VIP}}$  corresponding to  $\vec{w}_{nc}^{\text{VIP}}$ , we set the final  $\phi_n$  to the minimum of nodal values  $\phi_{nc}$  to satisfy condition (9) in all neighboring cells. Computation of a particular  $\phi_{nc}^{\text{VIP}}$  can be done in the following way. We denote reconstructed linear part of velocity  $\vec{u}_{nc} = \phi_n (\nabla \vec{w})_n (\vec{x}_c - \vec{x}_n)$ . This one is in limits if it lies in the convex hull (CH) of set

$$\text{CH}\{\vec{w}_m - \vec{w}_n, m \in N(c)\} = P_{nc}.$$

Polygon  $P_{nc}$  has one to four different vertices depending on the velocity field and contains the  $\vec{0}$  point. The zero velocity comes from bound in reconstruction center node and it represents piece-wise constant low-order reconstruction. Because of used linear reconstruction and because of scalar limiter  $\phi_{nc}$ , achievable reconstruction is located on a line segment from origin to  $\vec{u}_{nc}$ . Possible limiter values are represented by an intersection of this line segment with the convex

hull of  $P_{nc}$ . The best (least diffusive) limiter value  $\phi_n^c$  given by constraints in the cell center  $\vec{x}_c$  is the one closest to the  $\vec{u}_{nc}$  and corresponds to intersection  $\Phi_n^c$ .

To avoid construction of  $P_{nc}$  convex hull (CH), we discuss following two cases separately. We denote  $T_{nc} = \{P_{nc} \setminus \vec{0}\}$  which represents triangle of constrains. If  $\vec{0} \in T_{nc}$ , then the triangle is also boundary of  $P_{nc}$  convex hull and we can find  $\Phi_n^c$  as an intersection of the line segment with  $T_{nc}$ . If  $\vec{0} \notin T_{nc}$ , then computation of intersections  $\Psi_{nc}^i$  of  $T_{nc}$  with a ray from  $\vec{0}$  to  $\vec{u}_{nc}$  is also sufficient. If there is no intersection, then  $\vec{u}_{nc}$  points out of the CH and  $\Phi_n^c = \vec{0}$ . Otherwise  $\Phi_n^c = \min(1, \max_i(\Psi_{nc}^i))$ , where  $\max_i(\Psi_{nc}^i)$  returns intersection which is further from the origin (closer to  $\vec{u}_{nc}$ ). If it exists, second intersection  $\Psi_{nc}^i$  lies inside of the  $P_{nc}$  convex hull and therefore it is not interesting for us. To conclude, computation of intersection of a single ray with three line segments of  $T_{nc}$  is sufficient in both cases.

Let us project elements of  $T_{nc} = \{\vec{u}_{nc_i}, i \in \{1, 2, 3\}\}$  to the coordinate system given by  $\vec{u}_{nc} = \begin{pmatrix} u_{nc}^x \\ u_{nc}^y \end{pmatrix}$ , so

$$\vec{v}_{nc_i} = \frac{1}{|\vec{u}_{nc}|^2} \begin{pmatrix} u_{nc}^x & u_{nc}^y \\ -u_{nc}^y & u_{nc}^x \end{pmatrix} \vec{u}_{nc_i}. \quad (10)$$

After this projection, intersections have a simple form  $\Psi_{nc}^i = \begin{pmatrix} \psi_{nc}^i \\ 0 \end{pmatrix}$  and they are easy to find (11). Moreover, value  $\psi_{nc}^i$  now represents ratio of bound- and reconstructed- velocity linear parts, so this value is a candidate for the limiter in (5). It is only necessary to choose the correct intersection (12) as discussed above. Finally, minimal value from bounds in the four cells of node  $n$  is taken (13)

$$\psi_{nc}^i = v_{nc_i}^x + \frac{v_{nc_i}^y}{v_{nc_i}^y - v_{nc_{i+1}}^y} (v_{nc_{i+1}}^x - v_{nc_i}^x) \text{ if } v_{nc_i}^y v_{nc_{i+1}}^y < 0, \text{ else } \psi_{nc}^i = 0. \quad (11)$$

$$\phi_n^c = \min(1, \max_i(\psi_{nc}^i)). \quad (12)$$

$$\phi_n = \min_{c \in C(n)} (\phi_n^c). \quad (13)$$

Special care must be taken of when  $|\vec{u}_{nc}|^2$  or  $v_{nc_i}^y - v_{nc_{i+1}}^y$  are close to zero. Second case means that the line given by  $\vec{v}_{nc_i}, \vec{v}_{nc_{i+1}}$  is parallel to the ray or that our CH is only one point. It is sufficient to check if they are on or out of the axis. If they are out, we take zero limiter value, if they are on the axis, we simply take higher coordinate from the line endpoints. In a simple 1D case (constant velocity field along one direction), this limiter approaches standard 1D Barth-Jespersen method regardless of our special choice of bounds.

Application of the limited reconstruction for remapping is straightforward extension of the low-order method. Instead of using nodal values to compute momentum fluxes according to sign of corresponding mass flux, we simply use reconstructed velocity evaluated in the flux position. Note that in presence of discontinuity, the limiter value is zero and only bounds preserving donor fluxes are used.

In our particular implementation, remapping using piecewise linear velocity reconstruction with the VIP limiter is perfectly symmetric on a polar mesh, but there is small violation of bounds for a minimum of the radial velocity component, see fig. 3 (c). This undershoot was the main motivation for our novel corrected definition of vector bounds called Modified VIP (MVIP).

## 6. Modified VIP

The goal of this modification of the VIP method is a general correction which removes undershoot for the radial velocity component. Note that we can not directly limit this radial component, because is it not clear how to define radial direction for general vector field. Therefore, we add a new constraint for the minimal velocity magnitude (fig. 1 (d)) which is applied only in

situations where it is suitable. Imagine at first the situation with only two velocities in the opposite directions with the same magnitude. Then the VIP set is just a line segment and after the restriction on a minimal magnitude, we would not allow any contribution of any high-order term. This is an analog of 1D situation, where any magnitude smaller than the original one is acceptable. Analogous situation occurs in 2D when e.g. the origin of the coordinate system lies inside the CH of nodal velocities. Then it does not make a good sense to cut out a whole circle from the CH.

Therefore, we have decided to choose the following condition for application of the minimal magnitude correction of VIP. If we can find a rotated coordinate system in which all limiting velocities are located in one quadrant, then these velocities have a small angular discrepancy and the condition is applied. In more general case, we require limiting the angular discrepancy by any parameter  $\varphi_0$ . Our choice corresponds to  $\varphi_0 = \pi/2$ . In other words, for any pair of bounds-defining velocities, their dot product is positive. For the maximal velocity magnitude, we do not need to check this limit because velocities from VIP are always in bounds for the maximal magnitude.

Computation of the MVIP slope limiter extends the pure VIP to the following procedure. We evaluate the unlimited reconstruction in four cell centers that surround the node  $n$  (7, 8) and check limits for MVIP

$$\forall c \in C(n) \quad \vec{w}_{nc}^{\text{lim}} \in \text{MVIP}_c \quad (14)$$

where

$$\text{MVIP}_c = \begin{cases} \text{VIP}_c \cap \text{R}_c(0, \vec{w}^{\text{min}}) & \text{for } \forall n \in N(c), \forall m \in N(c) \quad \vec{w}_n \cdot \vec{w}_m > 0 \\ \text{VIP}_c & \text{otherwise,} \end{cases} \quad (15)$$

and where  $\text{VIP}_c$  represents the Convex Hull of nodal velocities  $\vec{w}_n$ ,  $n \in N(c)$ , and  $\text{R}_c(0, \vec{w}^{\text{min}}) = \{\vec{w}, |\vec{w}| \geq \min_{n \in N(c)} (|\vec{w}_n|)\}$ .

For a particular cell  $c$  attached to node  $n$ , we find at first maximal  $\phi_{nc} \in (0, 1)$  which keeps  $\vec{w}_{nc}^{\text{lim}}$  inside  $\text{VIP}_c$ . Let us call these  $\phi_{nc}^{\text{VIP}}$  and  $\vec{w}_{nc}^{\text{VIP}}$ . For a velocity field with a large angular discrepancy  $\text{MVIP}_c = \text{VIP}_c$  and therefore  $\phi_{nc} = \phi_{nc}^{\text{VIP}}$ . For a small one, check if limited velocity  $\vec{w}_{nc}^{\text{VIP}}$  lies also in  $\text{MVIP}_c$  and set

$$\phi_{nc} = \begin{cases} \phi_{nc}^{\text{VIP}} & \text{for } \vec{w}_{nc}^{\text{VIP}} \in \text{R}_c(0, \vec{w}^{\text{min}}) \\ \phi_{nc}^i & \text{otherwise,} \end{cases} \quad (16)$$

where  $\phi_{nc}^i$  is the limiter value corresponding to  $\vec{w}_{nc}^{\text{lim}}$  computed as the intersection of  $\text{R}_c(0, \vec{w}^{\text{min}})$  boundary with a line segment given by  $\vec{w}_n$  and  $\vec{w}_{nc}^{\text{VIP}}$ . Note that now  $\vec{w}_{nc}^{\text{VIP}}$  is not in  $\text{R}_c(0, \vec{w}^{\text{min}})$  (it is inside the circle given by its boundary) and clearly  $\vec{w}_n \in \text{R}_c(0, \vec{w}^{\text{min}})$ , so the intersection exists and it is unique,  $\phi_{nc}^i \in (0, \phi_{nc}^{\text{VIP}})$  and therefore  $\vec{w}_{nc}^{\text{lim}} \in \text{MVIP}_c$ .

Having computed all four  $\phi_{nc}$  corresponding to  $\vec{w}_{nc}^{\text{lim}}$ , we would like to set the final  $\phi_n$  to a minimum of nodal values  $\phi_{nc}$  to satisfy condition (14) in all neighboring cells. However,  $\text{MVIP}_c$ 's are not convex in general and therefore we need to check again  $\forall c \in C(n)$ , that the reconstructed velocities lie in  $\text{MVIP}_c$ . Let us note that

$$\phi_n^{\text{min}} = \min_{c \in C(n)} (\phi_{nc})$$

and  $\vec{w}_n^{\text{min}}(\vec{x}_c)$  is the reconstructed velocity corresponding to this limiter, finally

$$\phi_n = \begin{cases} \min_{c \in C(n)} (\phi_{nc}) & \text{for } \forall c \in C(n) \left( \vec{w}_n^{\text{min}}(\vec{x}_c) \in \text{R}_c(0, \vec{w}^{\text{min}}) \vee \forall (n, m) \in N(c) \quad \vec{w}_n \cdot \vec{w}_m \leq 0 \right) \\ 0 & \text{otherwise.} \end{cases} \quad (17)$$

The last choice of 0 for the limiter value could be replaced by a better choice. However, it would require multiple repetition of the whole procedure and the improvement of the method would not be significant.

An extension of our MVIP limiting method for polygonal mesh with any number of cell vertices is straightforward. The only difference is, that three line segments of  $T_{nc}$  components of which are used in (10) and represent 3 nodal velocities have to be replaced by line segments given by all pairs of all nodal velocities.

## 7. Numerical examples

A standard cyclic remapping method [10] was performed to verify properties of the described remapping techniques. Two kinds of prescribed grid motions are presented. First one is radially symmetric, so no motion in an angular and smooth one in a radial direction was used. Radial motion of a particular grid is given by

$$r(\xi, t) = (1 - \alpha(t))\xi + \alpha(t)\xi^3, \quad \alpha(t) = \frac{\sin(4\pi t)}{2}, \quad 0 \leq \xi \leq 1, \quad -1/8 \leq t \leq 1/8 \quad (18)$$

where  $\xi$  represents discrete value of relative nodal radius and  $t$  is the pseudotime. We use grids having 20/40/80 cells in radial and 40/80/160 cells in angular direction corresponding to 100/200/400 remaps. These grids were scaled to the computational domain  $(0.01, 0.51) \times (0, 2\pi)$ . Second grid motion is described at the end of this section.

### 7.1. Constant density and radial velocity on a polar grid

A simple initial conditions are given by constant density  $\rho = 1$  and radial velocity with step in magnitude  $|\vec{w}| = 1$  for  $r \geq 0.25$  and  $|\vec{w}| = 3$  for  $r < 0.25$ . Contour plots in Figure 2 correspond

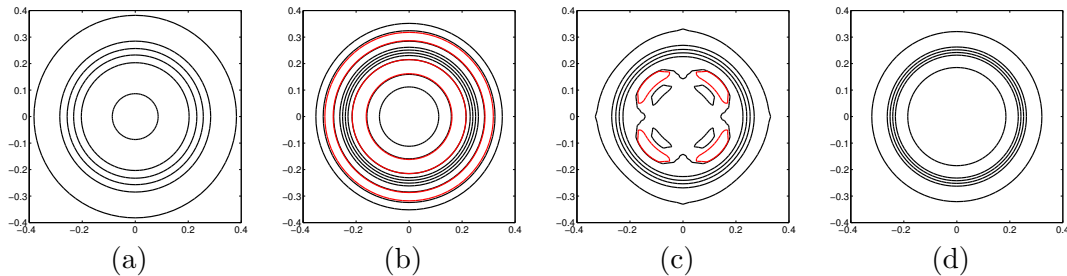


**Figure 2.** Contour plots of velocity magnitude for cyclic remapping of step in radial velocity field on a polar grid. (a) low-order, (b) unlimited, (c) BJ- and (d) MVIP-limited method.

to velocity magnitude of the remapped initial function. Red contours represent values out of bounds, namely 0.99 and 3.01. The figure clearly shows violation of symmetry by the Barth-Jespersen limiter. Figure 3 (a) shows the exact solution compared to the selected methods. BJ limited reconstruction leads to non-symmetric result. These results are in figure 3 (b, c) compared to VIP, resp. MVIP methods. The only difference between last two methods is visible in sub-figure (c), showing detail for minimal magnitude, where MVIP fixes small undershoot produced by the original VIP method.

To verify the order of accuracy of the MVIP method, we tried also a smooth function for radial velocity  $w_r(r) = \exp(-r)$  and again constant density. Table 1 shows second order of convergence for the new method.

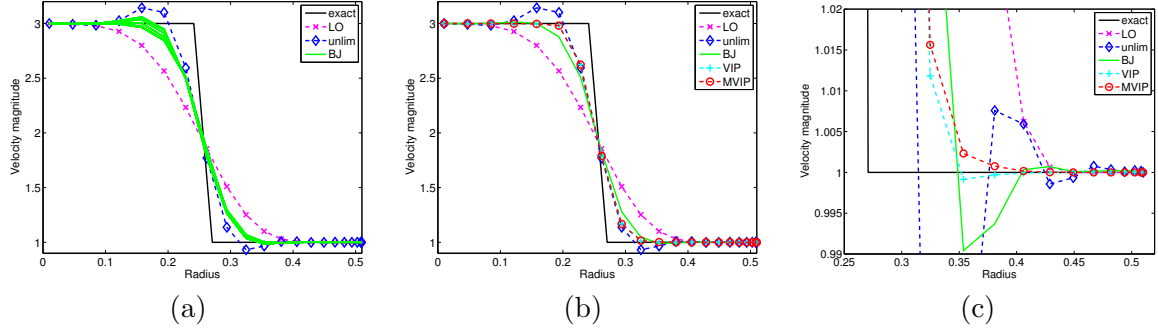


**Figure 3.** Scatter plots of velocity magnitude over angular direction. Subfigures (a, b) show the whole domain, where subfigures (b, c) show only one selected line for BJ-limiter and subfigure (c) discovers detail of the region with the minimal magnitude.

**Table 1.** Velocity  $L_1$  error and corresponding convergence rate for radial velocity  $w_r(r) = \exp(-r)$ . Methods with piece-wise constant (LO), unlimited-, resp. MVIP-limited piece-wise linear velocity reconstructions.

| remap | $E_{20 \times 40}$   | $E_{40 \times 80}$   | $E_{80 \times 160}$  | $\frac{20 \times 40}{40 \times 80}$ | $\frac{40 \times 80}{80 \times 160}$ |
|-------|----------------------|----------------------|----------------------|-------------------------------------|--------------------------------------|
| LO    | $6.19 \cdot 10^{-3}$ | $3.27 \cdot 10^{-3}$ | $1.67 \cdot 10^{-3}$ | 1.9                                 | 2.0                                  |
| unlim | $1.07 \cdot 10^{-3}$ | $2.68 \cdot 10^{-3}$ | $6.62 \cdot 10^{-5}$ | 4.0                                 | 4.0                                  |
| MVIP  | $1.59 \cdot 10^{-3}$ | $4.16 \cdot 10^{-4}$ | $1.07 \cdot 10^{-4}$ | 3.8                                 | 3.9                                  |

### 7.2. Noh-like problem on a polar grid

Initial conditions for density  $\rho$  and velocity  $\vec{w} = w_r(r) \begin{pmatrix} \cos \varphi \\ \sin \varphi \end{pmatrix}$  corresponding to an exact solution of the 2D Noh problem in selected time are

$$\rho(r) = \begin{cases} 16 & \text{for } r < 0.375 \\ 1 + 1.125/r & \text{for } r \geq 0.375 \end{cases}, \quad w_r(r) = \begin{cases} 0 & \text{for } r < 0.375 \\ -1 & \text{for } r \geq 0.375 \end{cases}.$$

Figure 4 (a) shows result for radial component of velocity (because of symmetry preservation of all methods, the absolute value of this component is equal to the velocity magnitude). Only the low-order and the MVIP methods keep the bounds. Convergence for this setup is shown in table 2.

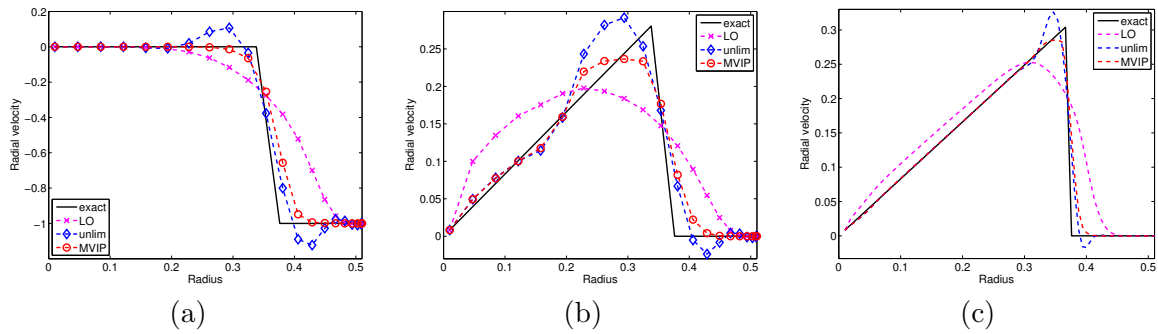


**Figure 4.** Radial velocity along radial direction for Noh-like (a). resp. Sedov-like (b,c) cyclic remapping on  $20 \times 40$  (a,b), resp.  $80 \times 160$  (c) cells.



**Table 2.** Velocity  $L_1$  error and corresponding convergence rate for Noh-like cyclic remapping.

| remap | $E_{20 \times 40}$   | $E_{40 \times 80}$   | $E_{80 \times 160}$  | $\frac{20 \times 40}{40 \times 80}$ | $\frac{40 \times 80}{80 \times 160}$ |
|-------|----------------------|----------------------|----------------------|-------------------------------------|--------------------------------------|
| LO    | $1.32 \cdot 10^{-1}$ | $9.73 \cdot 10^{-2}$ | $6.82 \cdot 10^{-2}$ | 1.4                                 | 1.4                                  |
| unlim | $6.47 \cdot 10^{-2}$ | $4.13 \cdot 10^{-2}$ | $2.65 \cdot 10^{-2}$ | 1.6                                 | 1.6                                  |
| MVIP  | $4.45 \cdot 10^{-2}$ | $2.70 \cdot 10^{-2}$ | $1.62 \cdot 10^{-2}$ | 1.6                                 | 1.7                                  |

### 7.3. Sedov-like problem on a polar grid

The last two tests use the initial conditions which are close to the solution of the Sedov problem

$$\rho(r) = \begin{cases} 6 \left( \frac{r}{0.375} \right)^8 & \text{for } r < 0.375 \\ 1 & \text{for } r \geq 0.375 \end{cases}, \quad w_r(r) = \begin{cases} 0.83r & \text{for } r < 0.375 \\ 0 & \text{for } r \geq 0.375 \end{cases}, \quad (19)$$

where  $r = \sqrt{(x - x_0)^2 + (y - y_0)^2}$  and  $x_0 = y_0 = 0$ . Results on the polar grid are shown in figure 4 (b, c) for two different grids. MVIP again preserve bounds and symmetry.

### 7.4. Sedov-like problem on a Cartesian grid

This cyclic remapping test is similar to [15]. The initial condition is the same as previous, but  $x_0 = y_0 = 0.5$  in (19). We present results in half-time compared to the original paper. This pseudo-time corresponds to the maximal deformation of the grid. Our selection was motivated by the fact that some truncation errors may cancel during backward mesh movement [16]. Cartesian grid with  $64 \times 64 / 128 \times 128 / 256 \times 256$  initially equidistantly spaced cells was used and 160/320/640 remaps were performed. Grid movement is given by

$$x(\xi, \eta, t) = \xi + t \sin(2\pi\xi) \sin(2\pi\eta), \quad (20)$$

$$y(\xi, \eta, t) = \eta + t \sin(2\pi\xi) \sin(2\pi\eta), \quad 0 \leq \xi \leq 1, \quad 0 \leq \eta \leq 1, \quad 0 \leq t \leq 0.25, \quad (21)$$

where  $\xi, \eta$  represent discrete position in x,y plane and  $t$  is the discrete pseudotime. Table 3 shows convergence of the selected methods and symmetry of the remapped radial velocity component is compared in figure 5. Red contours (starting on value -0.01) represent undershoots in radial velocity. Note that the MVIP method keeps symmetry better than pure low-order or unlimited method even for non-symmetric mesh movement.

**Table 3.** Velocity  $L_1$  error and corresponding convergence rate for Sedov-like cyclic remapping.

| remap | $E_{64^2}$           | $E_{128^2}$          | $E_{256^2}$          | $\frac{64^2}{128^2}$ | $\frac{128^2}{256^2}$ |
|-------|----------------------|----------------------|----------------------|----------------------|-----------------------|
| LO    | $2.32 \cdot 10^{-2}$ | $1.63 \cdot 10^{-2}$ | $1.12 \cdot 10^{-2}$ | 1.4                  | 1.5                   |
| unlim | $1.30 \cdot 10^{-2}$ | $7.78 \cdot 10^{-3}$ | $4.70 \cdot 10^{-3}$ | 1.7                  | 1.7                   |
| MVIP  | $1.37 \cdot 10^{-2}$ | $8.21 \cdot 10^{-3}$ | $4.84 \cdot 10^{-3}$ | 1.7                  | 1.7                   |

## 8. Conclusions

In this paper, we have presented a significant modification of the Vector Image Polygon (VIP) limiter for a piece-wise linear velocity reconstruction. Resulting remap of momentum and

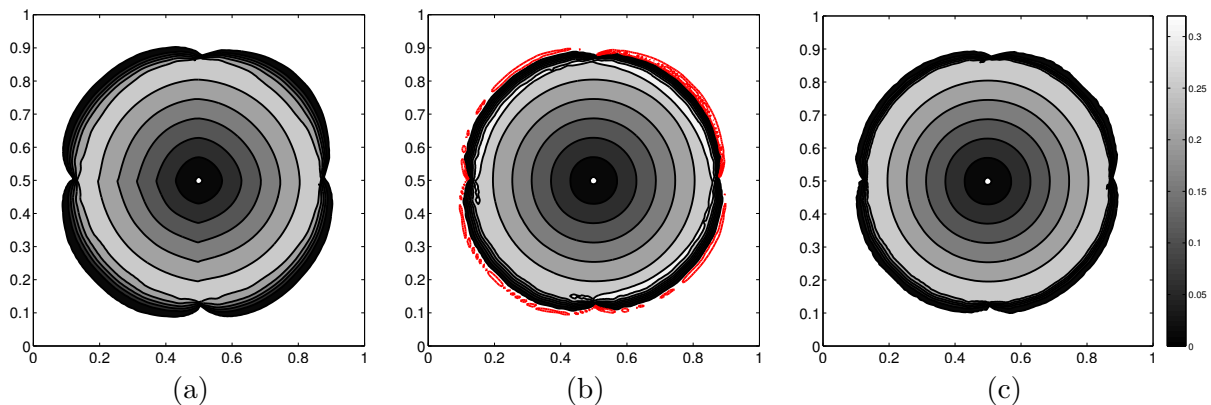


**Figure 5.** Contour plots of radial velocity component for cyclic remapping on a Cartesian grid. (a) low-order, (b) unlimited and (c) MVIP-limited method.

corresponding velocity are symmetric. Compared to the standard VIP method, the Modified VIP (MVIP) method shows local-bound preservation even for vector magnitude. However, there are still unresolved issues related to poor convergence for a case of small velocity gradients corresponding to almost constant fields on angularly under-resolved meshes. In this case, the VIP as well as MVIP limitations seem to be over-restrictive, which results in only first-order of convergence. We are also working on an alternative symmetry-preserving remap of momentum based on Flux Corrected Transport (FCT) ideas which overcomes this issue. Still, the Modified VIP method seems to be promising for application in ALE hydrodynamical codes.

### Acknowledgments

This work was performed under the auspices of the National Nuclear Security Administration US DOE at LANL under Contract No. DE-AC52-06NA25396, and partially supported by ASCR and ASC Programs, the CTU grant SGS10/299/OHK4/3T/14, the Czech Science Foundation projects P205/10/0814 and by the Czech Ministry of Education project RVO 68407700.

### References

- [1] Hirt C W, Amsden A A and Cook J L 1974 *Journal of Computational Physics* **14** 227–253
- [2] Liska R *et al.* 2011 *Finite Volumes for Complex Applications VI Problems & Perspectives* **4** 857–873
- [3] Galera S, Maire P H and Breil J 2010 *Computers & Fluids* **46** 161–167
- [4] Barlow A J 2008 *International Journal for Numerical Methods in Fluids* **56** 953–964
- [5] Burton D E 1994 Consistent finite-volume discretization of hydrodynamics conservation laws for unstructured grids Tech. rep. LLNL UCRL-JC-118788
- [6] Robinson A C *et al.* 2008 *Proceedings of the 46th AIAA Aerospace Sciences Meeting* AIAA-2008-1235
- [7] Anderson R W, Elliott N S and Pember R B 2004 *Journal of Computational Physics* **199** 598–617
- [8] Luttwak G and Falcovitz J 2011 *International Journal for Numerical Methods in Fluids* **65** 1365–1375
- [9] Maire P H 2011 Contribution to the numerical modeling of inertial confinement fusion UB I, Habilitation.
- [10] Margolin L G and Shashkov M 2003 *Journal of Computational Physics* **184** 266–298
- [11] Pember R B and Anderson R W 2000 A comparison of staggered-mesh Lagrange plus remap and cell-centered direct Eulerian Godunov schemes for Eulerian shock hydrodynamics Tech. rep. LLNL UCRL-JC-139820
- [12] DeBar R B 1974 Fundamentals of the KRAKEN code Tech. Rep. UCIR-760 Lawrence Livermore Laboratory
- [13] Barth T and Jespersen D 1989 The design and application of upwind schemes on unstructured meshes Tech. Rep. AIAA-89-0366 AIAA, NASA Ames Research Center
- [14] Maire P H, Loubère R and Váchal P 2011 *Commun. Comput. Phys.* **10** 940–978
- [15] Liska R, Shashkov M, Váchal P and Wendroff B 2010 *Journal of Computational Physics* **229** 1467–1497
- [16] Velechovsky J, Liska R and Shashkov M 2012 *Computers & Fluids* In press, <http://dx.doi.org/10.1016/j.compfluid.2012.06.006>